

DEEP OPTICAL PHOTOMETRY OF SIX FIELDS IN THE ANDROMEDA GALAXY¹

THOMAS M. BROWN², ED SMITH², HENRY C. FERGUSON², PURAGRA GUHATHAKURTA³, JASON S. KALIRAI², RANDY A. KIMBLE⁴,
ALVIO RENZINI⁵, R. MICHAEL RICH⁶, ALLEN V. SWEIGART⁴, DON A. VANDENBERG⁷

Accepted for publication in The Astrophysics Journal Supplement Series

ABSTRACT

Using the Advanced Camera for Surveys on the *Hubble Space Telescope*, we have obtained deep optical images reaching well below the oldest main sequence turnoff in six fields of the Andromeda Galaxy. The fields fall at four positions on the southeast minor axis, one position in the giant stellar stream, and one position on the northeast major axis. These data were obtained as part of three large observing programs designed to probe the star formation history of the stellar population in various structures of the galaxy. In this paper, we present the images, catalogs, and artificial star tests for these observing programs as a supplement to the analyses published previously. These high-level science products are also archived at the Multimission Archive at the Space Telescope Science Institute.

Subject headings: galaxies: evolution – galaxies: stellar content – galaxies: individual (M31)

1. INTRODUCTION

The Andromeda Galaxy (M31) is an ideal laboratory for testing theories of spiral galaxy formation and evolution. It appears to be representative of giant spiral galaxies in the nearby universe (Hammer et al. 2007), and it is the only giant spiral galaxy where we can accurately measure the complete star formation history from an external vantage point, using photometry reaching below the oldest turnoff on the stellar main sequence. Using the Advanced Camera for Surveys (ACS) on the *Hubble Space Telescope* (HST), we obtained deep optical photometry of six fields in M31 (Figure 1), with which we reconstructed the star formation history at various points in the spheroid, disk, and giant stellar stream (Brown et al. 2003, 2006, 2007, 2008). As a supplement to those studies, we present in this paper the reduced images and their associated photometric catalogs, along with characterizations of the photometric scatter and completeness derived from artificial star tests. These high-level science products (HLSPs) can facilitate comparison with other studies of stellar populations in nearby galaxies or aid in the planning of additional observations in Andromeda itself.

2. OBSERVATIONS AND DATA REDUCTION

The characteristics of the six fields shown in Figure 1 are summarized in Table 1. Images were obtained using the Wide Field Camera on the ACS, in the F606W (broad V) and F814W (I) filters. These data were obtained as part of three Large (> 100 orbits) Guest Observer (GO) programs (GO-

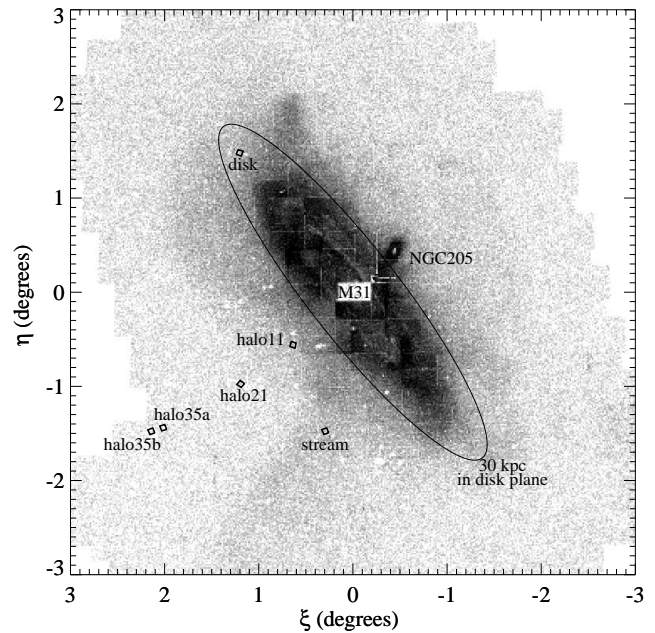


FIG. 1.— The stellar density in the Andromeda vicinity, from counts of RGB stars (Ferguson et al. 2002). Our six fields are indicated (*labeled boxes*). An ellipse marks the area within 30 kpc of the galactic center in the inclined disk plane (*labeled*). Later surveys that go wider and deeper (e.g., Ibata et al. 2007) show an even greater wealth of substructure in the system.

9453, GO-10265, and GO-10816) in *HST* Observing Cycles 11, 13, and 15.

The data properties are not uniform across observing cycles. The primary distinction is that each program obtained systematically shallower images than the preceding one. When the original program was planned for the halo11 field, no images of M31 had reached significantly below the luminosity of the horizontal branch, let alone the main sequence turnoff. Given the uncertainties, the original program was designed to reach 1.5 mag below the oldest main sequence turnoff that might be present, in order to ensure an unambiguous characterization of the detailed star formation history. The position of the halo11 field on the minor axis was chosen to optimize the crowding (trading population sample size against photometric uncertainties). In addition, the

¹ Based on observations made with the NASA/ESA *Hubble Space Telescope*, obtained at the Space Telescope Science Institute, which is operated by the Association of Universities for Research in Astronomy, Incorporated, under NASA contract NAS5-26555.

² Space Telescope Science Institute, Baltimore, MD 21218; tbrown@stsci.edu, edsmith@stsci.edu, ferguson@stsci.edu, jkalirai@stsci.edu

³ University of California Observatories / Lick Observatory, University of California, Santa Cruz, CA 95064; raja@ucolick.org

⁴ NASA Goddard Space Flight Center, Greenbelt, MD 20771; randy.a.kimble@nasa.gov, allen.v.sweigart@nasa.gov

⁵ Osservatorio Astronomico, I-35122 Padova, Italy; alvio.renzini@oapd.inaf.it

⁶ Department of Physics and Astronomy, University of California, Los Angeles, CA 90095; rmr@astro.ucla.edu

⁷ Department of Physics and Astronomy, University of Victoria, P.O. Box 3055, Victoria, BC, V8W 3P6, Canada; vandenbe@uvic.ca

TABLE 1
CHARACTERISTICS OF M31 FIELDS

Field	Program Number	R.A. (J2000)	Dec. (J2000)	F606W (ksec)	F814W (ksec)	Date
halo11	GO-9453	00:46:07.1	40:42:39	138.6	161.3	2 Dec 2002 – 1 Jan 2003
stream	GO-10265	00:44:18.2	39:47:32	52.8	78.1	30 Aug 2004 – 4 Oct 2004
disk	GO-10265	00:49:08.6	42:45:02	52.8	78.1	11 Dec 2004 – 18 Jan 2005
halo21	GO-10816	00:49:05.1	40:17:32	28.7	47.8	9 Aug 2006 – 28 Aug 2006
halo35a	GO-10816	00:53:28.1	39:49:46	28.1	46.9	12 Oct 2006 – 18 Oct 2006
halo35b	GO-10816	00:54:08.5	39:47:26	28.1	51.6	18 Oct 2006 – 6 Jan 2007

halo11 field was chosen to be in the vicinity of other historical probes of the M31 spheroid. From an analysis of subsets of the data from the original program (GO-9453), we were able to empirically determine how the fidelity of the recovered star formation history depended upon the depth of the photometry. This analysis showed that a depth of 1 mag below the oldest main sequence turnoff was sufficient to characterize the star formation history. By using this shallower depth in our second program (GO-10265), we were able to determine the star formation history in two fields without increasing the overall size of the observing program. As with the first program, the locations of the fields within the targeted structures (disk and giant stellar stream) were again chosen to provide near-optimal levels of crowding. In contrast, the third program (GO-10816) targeted regions of the M31 spheroid far sparser than those in the first two programs. Because it was necessary to trade depth against the number of fields to ensure an adequate sample size, the third program was designed to reach 0.8 mag below the oldest main sequence turnoff in each of its fields.

Besides the above differences in the photometric depth between programs, there were also differences among the fields of the third program. That program planned to obtain one halo field at 21 kpc and three halo fields at 35 kpc along the minor axis, thereby providing approximately the same number of stars in each of these two locations. Due to a hardware failure in the ACS during Cycle 15, the third program was terminated before it obtained any observations in the final 35 kpc field, and so the sample size at 35 kpc is approximately 2/3 of that at 21 kpc. Furthermore, one of the fields in the third program (halo35b) had significant deviations from the planned F814W exposures. Guide star problems caused some exposures to fail outright and other exposures to be significantly offset ($\sim 80''$) from the planned pointing. The problematic exposures were rescheduled with a 102° change in orientation.

Our reduction process for the first two programs was fully documented in Brown et al. (2006), to which we refer readers for details. Note that the catalog produced by Brown et al. (2006) for the halo11, stream, and disk fields was subject to more rigorous detection thresholds and culling procedures than that produced by Brown et al. (2003) for the halo11 field; while the earlier catalog is thus deeper, it also included more spurious sources. The reduction for the subsequent fields (halo21, halo35a, and halo35b) was documented in Brown et al. (2007, 2008). The process used in the later fields was similar to that in Brown et al. (2006), with the additional correction for charge transfer inefficiency (CTI). A CTI correction was unnecessary for the photometry in the first two programs, given the crowded field, high background, and relative youth of the detector.

We briefly summarize the reduction process here. The individual exposures for each bandpass in a given field were registered using the positions of bright stars well-detected in each exposure. The exposures were then combined using the

DRIZZLE package (Fruchter & Hook 2002), including correction for geometric distortion, rescaling to $0.03''$ pixel $^{-1}$, and rejection of cosmic rays and hot pixels. The individual frames in each field were drizzled to a 7500×7500 pixel output image, and then this output image was cropped to a 7000×7350 pixel image with the World Coordinate System in the header intact. As part of this process, the sky background was subtracted from individual frames prior to drizzling (to avoid increasing the noise in a process that essentially interlaces the individual frames), and then the sky background was restored to the coadded images (to ensure that the counting statistics in subsequent object detection and photometry routines were appropriate). PSF-fitting photometry was then performed with the DAOPHOT-II software of Stetson (1987). The PSF-fitting photometry was corrected to agree with aperture photometry of isolated stars, with the zeropoints calibrated at the 1% level. For the fields in the third program, the CTI correction of Riess & Mack (2005) was applied. Our photometry is in the STMAG system: $m = 2.5 \log_{10} f - 21.1$ mag, where $f = e^{-\text{PHOTFLAM} \times \text{EXPTIME}}$, where EXPTIME is the exposure time, and PHOTFLAM is $7.906 \times 10^{-20} \text{ erg s}^{-1} \text{ cm}^{-2} \text{ \AA}^{-1} / (e^{-1} \text{ s}^{-1})$ for the F606W filter and $7.072 \times 10^{-20} \text{ erg s}^{-1} \text{ cm}^{-2} \text{ \AA}^{-1} / (e^{-1} \text{ s}^{-1})$ for the F814W filter. For those more familiar with the ABMAG system, $\text{ABMAG} = \text{STMAG} - 0.169$ for m_{F606W} , and $\text{ABMAG} = \text{STMAG} - 0.840$ mag for m_{F814W} .

Note that Brown et al. (2006) shifted the stream photometry 0.03 mag brighter in m_{F814W} and 0.014 mag redder in $m_{F606W} - m_{F814W}$ color. These shifts produced excellent agreement between the distributions of stars on the horizontal branch and red giant branch (RGB) in the halo11 and stream fields. The shift in brightness is justified by the fact that the stream is located behind Andromeda (McConnachie et al. 2003), while the shift in color is well within the calibration and reddening uncertainties. The stream catalog presented here does not include these shifts in color and magnitude.

The catalogs were then culled to remove problematic stars (artifacts, blends, extended objects, etc.) using object sharpness, proximity to brighter stars, and the map of underexposed areas in the image (due to dithering the image edges and the detector gap). In the halo11 field, stars within 500 pixels ($15''$) of the globular cluster GC312 were also removed from the catalog. This radius was chosen to safely exceed the cluster's tidal radius of $10''$ (Holland et al. 1997); the deep photometry of GC312 was analyzed separately by Brown et al. (2004). Given the problems with the 35 kpc sample (one field missing outright and another field with pointing irregularities in the F814W band), an exception was made to the culling process for the halo35b field to maximize the number of stars in the 35 kpc sample. Instead of culling any stars falling in a part of the image with off-nominal exposure time, we included regions where the exposure depth was within 0.2 mag of nominal; this includes regions of the image that are 0.1 mag deeper

TABLE 2
CATALOG FOR HALO11 FIELD

x (pixels)	y (pixels)	R.A. (J2000)	Dec. (J2000)	m_{F606W} (mag)	m_{F606W} error (mag)	m_{F814W} (mag)	m_{F814W} error (mag)
65.11	310.17	00:46:00.99	+40:40:28.20	28.98	0.04	29.35	0.06
65.61	313.96	00:46:01.00	+40:40:28.24	30.18	0.12	30.20	0.09
132.41	314.27	00:46:00.96	+40:40:30.18	31.08	0.25	31.07	0.18
144.49	315.30	00:46:00.95	+40:40:30.54	30.43	0.13	30.39	0.08
269.93	314.81	00:46:00.86	+40:40:34.17	28.46	0.03	28.92	0.03

Only a portion of this table is shown here to demonstrate its form and content.
A machine-readable version of the full table is available.

TABLE 3
CATALOG FOR STREAM FIELD

x (pixels)	y (pixels)	R.A. (J2000)	Dec. (J2000)	m_{F606W} (mag)	m_{F606W} error (mag)	m_{F814W} (mag)	m_{F814W} error (mag)
34.30	312.88	00:44:12.71	+39:49:46.58	28.98	0.06	29.52	0.06
179.08	318.11	00:44:13.06	+39:49:44.81	29.21	0.07	29.65	0.08
171.98	318.93	00:44:13.04	+39:49:44.87	28.44	0.05	28.98	0.04
35.41	320.12	00:44:12.71	+39:49:46.37	29.23	0.07	29.68	0.09
217.24	320.04	00:44:13.15	+39:49:44.33	30.33	0.21	30.88	0.25

Only a portion of this table is shown here to demonstrate its form and content.
A machine-readable version of the full table is available.

TABLE 4
CATALOG FOR DISK FIELD

x (pixels)	y (pixels)	R.A. (J2000)	Dec. (J2000)	m_{F606W} (mag)	m_{F606W} error (mag)	m_{F814W} (mag)	m_{F814W} error (mag)
47.06	311.27	00:49:04.00	+42:42:41.95	29.61	0.08	29.79	0.07
229.83	314.39	00:49:03.82	+42:42:47.03	27.92	0.03	28.46	0.03
134.46	315.17	00:49:03.92	+42:42:44.41	29.89	0.13	30.09	0.10
170.79	316.31	00:49:03.88	+42:42:45.43	29.18	0.07	29.84	0.10
91.33	318.42	00:49:03.97	+42:42:43.26	29.12	0.07	29.66	0.08

Only a portion of this table is shown here to demonstrate its form and content.
A machine-readable version of the full table is available.

than planned (approximately 50% of the image area) and regions that are 0.2 mag shallower than planned (approximately 10% of the image area). Even though much of the halo35b F814W image is deeper than planned, the sky background for the field is also higher than that in the halo35a field, because it executed later in the year, when the Sun angle for Andromeda was smaller.

To characterize the scatter and incompleteness in the photometric catalogs, thousands of artificial star tests were performed on the images from each field; each test inserted and blindly recovered hundreds to thousands of stars, but the total number of artificial stars tested in each field exceeded 4 million. The artificial star tests were uniformly distributed over the regions of each image spanned by its associated catalog. For the halo35b field, the stars were inserted and recovered in a manner consistent with the varying exposure depth in the image (i.e., with stellar magnitudes scaled to the exposure time of the region where the stars were inserted).

3. HIGH-LEVEL SCIENCE PRODUCTS

The HLSPs include coadded images, masks, catalogs, and artificial star tests. All of these products have been delivered to the Multimission Archive at the Space Telescope Science Institute (MAST). The catalogs are also in-

cluded as electronic tables here (Tables 2–7) with their own naming convention specific to the Journal. The HLSPs follow the MAST naming convention. Each filename begins with `hlsp_andromeda_hst_acs-wfc_`, concatenating `hlsp` with the project name, mission name, and instrument name. The remainder of the filename concatenates the field name (given in Table 1), the relevant filter(s), the version number, the product type, and a suffix. The version number for the products discussed here is `v2`, because the process we developed was changed significantly between Brown et al. (2003) and Brown et al. (2006). The product types are images (`img`), masks (`msk`), catalogs (`cat`), and artificial star tests (`art`). The catalogs are ascii machine-readable tables with suffix `txt`, while the remaining products are FITS files with suffix `fits`. All of the FITS files are in standard FITS format without multiple FITS extensions.

Each field has two coadded images – one for each band (F606W and F814W). The floating-point array in each file is in units of counts, with all parts of each image scaled to a common exposure time (given by the `EXPTIME` keyword in the image header and in Table 1). The geometric distortion in the ACS is significant, such that there is an irregular border of unexposed pixels in each rectangular image after correction for geometric distortion. This border has been set to a value of

TABLE 5
CATALOG FOR HALO21 FIELD

x (pixels)	y (pixels)	R.A. (J2000)	Dec. (J2000)	m_{F606W} (mag)	m_{F606W} error (mag)	m_{F814W} (mag)	m_{F814W} error (mag)
280.50	233.02	00:49:06.77	+40:19:57.06	29.89	0.17	30.18	0.19
765.69	249.27	00:49:07.52	+40:19:45.29	27.65	0.04	28.02	0.03
528.11	253.14	00:49:07.13	+40:19:50.83	29.53	0.11	30.14	0.17
379.68	253.21	00:49:06.89	+40:19:54.34	29.08	0.07	29.54	0.07
623.00	253.86	00:49:07.28	+40:19:48.58	29.62	0.15	30.04	0.11

Only a portion of this table is shown here to demonstrate its form and content.
A machine-readable version of the full table is available.

TABLE 6
CATALOG FOR HALO35A FIELD

x (pixels)	y (pixels)	R.A. (J2000)	Dec. (J2000)	m_{F606W} (mag)	m_{F606W} error (mag)	m_{F814W} (mag)	m_{F814W} error (mag)
427.99	229.71	00:53:17.44	+39:50:58.61	28.91	0.08	29.48	0.10
145.40	230.58	00:53:16.74	+39:50:56.24	29.17	0.10	29.65	0.11
1214.17	237.96	00:53:19.42	+39:51:04.88	29.31	0.10	29.92	0.14
1049.68	239.57	00:53:19.01	+39:51:03.47	29.23	0.10	29.89	0.11
1538.71	245.01	00:53:20.24	+39:51:07.37	29.12	0.10	29.52	0.10

Only a portion of this table is shown here to demonstrate its form and content.
A machine-readable version of the full table is available.

TABLE 7
CATALOG FOR HALO35B FIELD

x (pixels)	y (pixels)	R.A. (J2000)	Dec. (J2000)	m_{F606W} (mag)	m_{F606W} error (mag)	m_{F814W} (mag)	m_{F814W} error (mag)
50.27	221.81	00:53:56.66	+39:48:30.44	28.46	0.06	28.83	0.06
906.23	228.29	00:53:58.78	+39:48:38.32	28.53	0.06	28.75	0.05
509.27	228.74	00:53:57.80	+39:48:34.57	28.38	0.06	28.68	0.06
502.70	244.08	00:53:57.80	+39:48:34.07	29.98	0.16	29.55	0.08
1567.05	250.23	00:54:00.43	+39:48:43.92	28.91	0.07	29.43	0.10

Only a portion of this table is shown here to demonstrate its form and content.
A machine-readable version of the full table is available.

3×10^7 counts so that it can be easily masked in image analysis software. There are also a handful of negative pixels near this border – an artifact of the DRIZZLE process in places where the image is severely underexposed.

Associated with each field is a mask file. The byte array in each mask file is set to 0 in regions of the image valid for the catalog and artificial star tests, and set to 1 in regions that are invalid. The masking in these files is much more aggressive than that given by the pixels set to 3×10^7 counts in the coadded images described above, since the latter is merely intended to flag pixels with little or no exposure time. Here, the mask is set to 0 where the exposure time deviates significantly from the planned exposure time due to dithers.

The catalogs for each field have 8 columns: x (pixels, 1-indexed), y (pixels, 1-indexed), right ascension (J2000), declination (J2000), m_{F606W} (magnitudes), m_{F606W} error (magnitudes), m_{F814W} (magnitudes), and m_{F814W} error (magnitudes). The error reported in the catalogs is simply that given by DAOPHOT-II. We do not use these errors in our own analyses; instead, when comparing models to the data, we scatter our models according to the results of artificial star tests. The right ascension and declination for each star comes from the World Coordinate System specified in the image headers, and is only as accurate as the coordinates of the guide stars used

in the observations. The first two programs executed with the first version of the Guide Star Catalog, with an associated astrometric uncertainty of 1° ; the third program executed with the second version of the Guide Star Catalog, with an associated astrometric uncertainty of 0.3° . Truncated versions of the catalog for each field are provided in Tables 2–7. The full catalog for each field is provided as a machine-readable electronic table in the online edition of The Astrophysical Journal. Binned versions of all six catalogs are shown in Figure 2.

The artificial star tests are provided as 4-dimensional floating-point arrays. These arrays give the scattering kernel at each point in the color-magnitude diagram (CMD). Examples of these scattering kernels are given in Figure 3. The first dimension of the array is the input $m_{F606W} - m_{F814W}$ color, binned from -1.1 mag to 0.4 mag with 16 steps of 0.1 mag. The second dimension of the array is the input m_{F814W} magnitude, binned from 31.5 mag to 22.5 mag with 91 steps of 0.1 mag. The third dimension of the array is the output $m_{F606W} - m_{F814W}$ color relative to the input color, binned from -0.51 mag to 0.51 mag with 51 steps of 0.02 mag. The fourth dimension of the array is the output m_{F814W} magnitude relative to the input magnitude, binned from -0.51 mag to 0.51 mag with 51 steps of 0.02 mag. To avoid confusion, it is worth stressing the sign convention in the second and

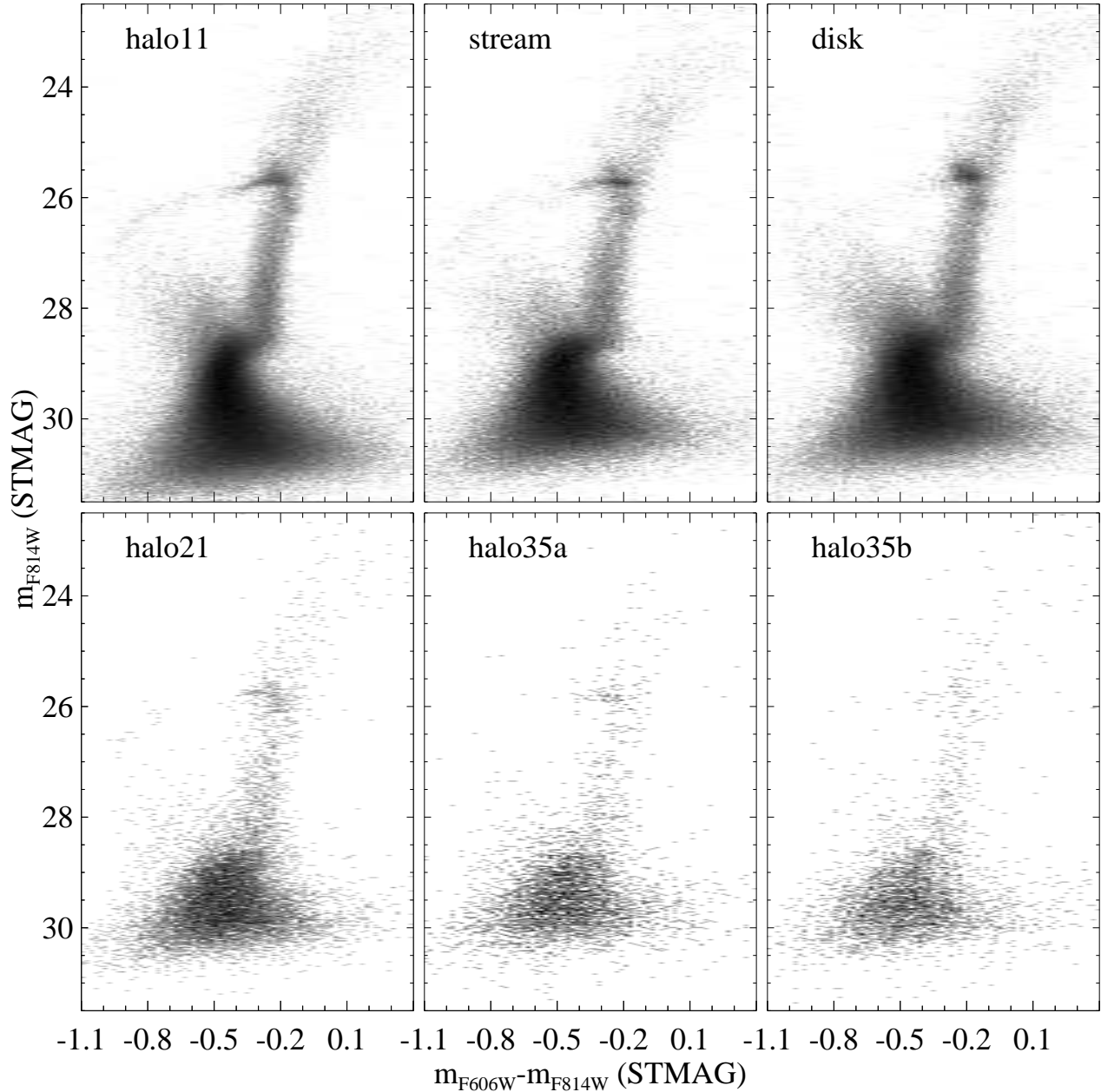


FIG. 2.— The binned color-magnitude diagrams for the six fields given in Table 1, shown at a logarithmic stretch.

fourth dimensions reflects that in the astronomical magnitude system. The output scattering kernel (i.e., the third and fourth dimensions of the array) is normalized such that the sum of the elements gives the completeness. The scattering kernel is slowly varying on the scale of the input binning (0.1 mag), while the binning of the scattering kernel itself (0.02 mag) matches the scale used to compare data and models in our star formation history analyses (Brown et al. 2006, 2007, 2008).

For example, using a 1-indexed system, the elements in the artificial star test arrays that correspond to (5,21,*,*) give the scattering kernel for artificial stars input at colors within 0.05 mag of $m_{F606W} - m_{F814W} = 0.7$ mag and magnitudes within 0.05 mag of $m_{F814W} = 29.5$ mag. The sum of these elements in the halo11 field is 0.895, implying that the completeness for stars at this color and magnitude is 89.5%. This scattering kernel is displayed in the lower left-hand panel of Figure 3.

4. SUMMARY

In this paper, we have made public the HLSPs associated with three *HST* Large GO programs targeting various structures in the giant spiral galaxy M31. The deep images and their associated masks, catalogs, and artificial star tests have been delivered to the MAST archive, at the same site used to store HLPs from *HST* Treasury programs. The catalogs are also available as electronic tables in this paper. The information provided should be sufficient to make detailed comparisons between the data in our observing programs and data in other programs targeting nearby stellar populations.

Support for Programs GO-9453, GO-10265, and GO-10816 was provided by NASA through a grant from the Space Telescope Science Institute, which is operated by the Association of Universities for Research in Astronomy, Incorpo-

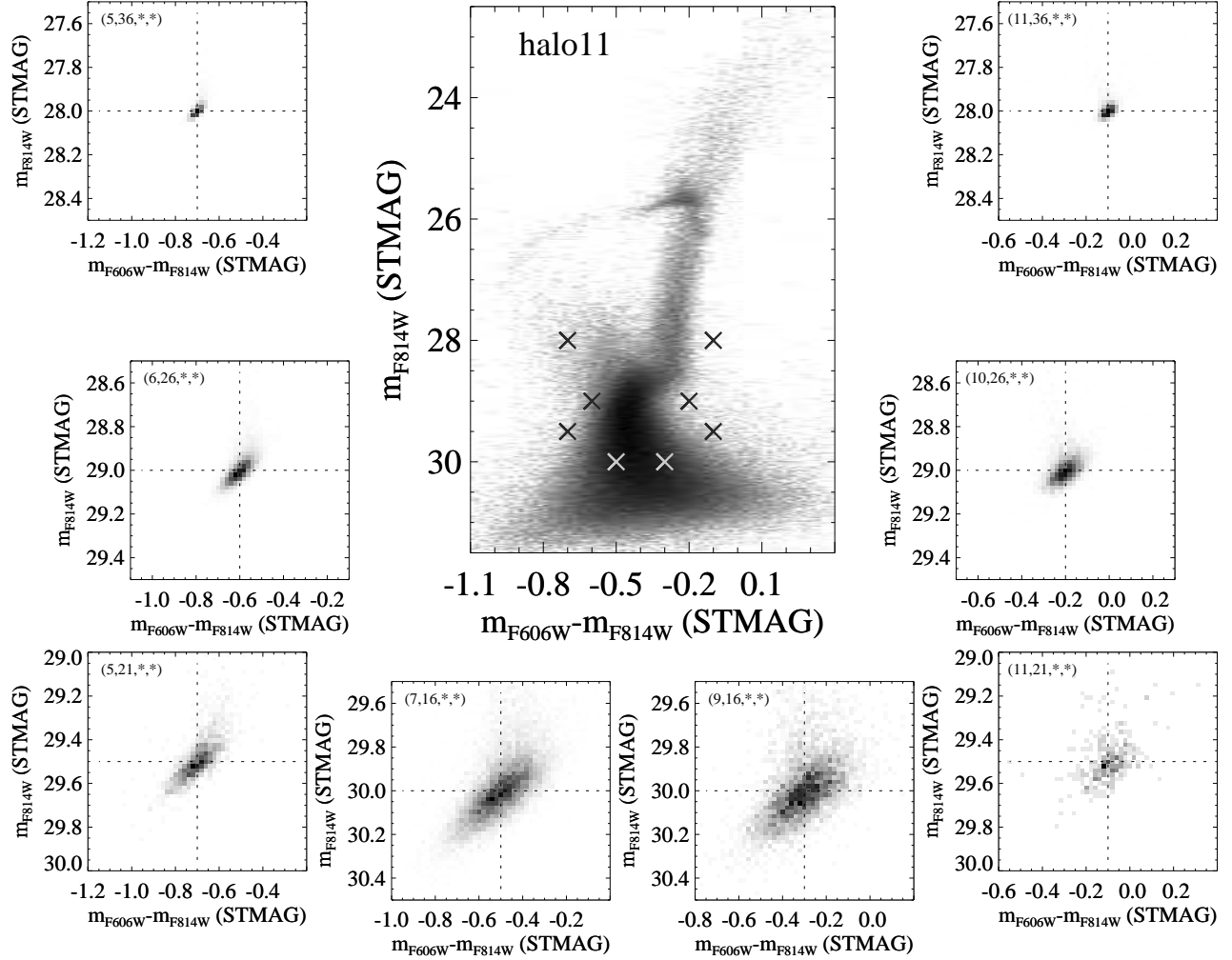


FIG. 3.— The binned CMD for the halo11 field (*large central panel*), with the scattering kernels (*small panels*) corresponding to 8 locations in the CMD (grey crosses). Each scattering kernel is labeled with the corresponding indices in the artificial star test arrays. The CMD and scattering kernels are shown at a logarithmic stretch.

rated, under NASA contract NAS5-26555. P. Royle and S. Meyett were enormously helpful in the scheduling and execution of these Large *HST* programs. PG and JSK would like to acknowledge support from NASA grants associated with these *HST* programs and from the following NSF grants

to UCSC: AST-0307966, AST-0507483, and AST-0607852. RMR would like to acknowledge support from grants associated with these *HST* programs and also NSF-AST-03-07931. We are grateful to P. Stetson for his DAOPHOT code.

REFERENCES

- Brown, T.M., et al. 2007, *ApJ*, 658, L95
 Brown, T.M., et al. 2008, *ApJ*, 685, L121
 Brown, T.M., Ferguson, H.C., Smith, E., Kimble, R.A., Sweigart, A.V., Renzini, A., Rich, R.M., & Vandenberg, D.A. 2003, *ApJ*, 592, L17
 Brown, T.M., Ferguson, H.C., Smith, E., Kimble, R.A., Sweigart, A.V., Renzini, A., Rich, R.M., & Vandenberg, D.A. 2004, *ApJ*, 613, L125
 Brown, T.M., Smith, E., Ferguson, H.C., Rich, R.M., Guhathakurta, P., Renzini, A., Sweigart, A.V., & Kimble, R.A. 2006, *ApJ*, 652, 323
 Ferguson, A.M.N., Irwin, M.J., Ibata, R.A., Lewis, G.F., & Tanvir, N.R. 2002, *AJ*, 124, 1452
 Fruchter, A.S., & Hook, R.N. 2002, *PASP*, 114, 144
 Hammer, F., Puech, M., Chemin, L., Flores, H., & Lehnert, M.D. 2007, *ApJ*, 662, 322
 Holland, S., Fahlman, G.G., & Richer, H.B. 1997, *AJ*, 114, 1488
 Ibata, R., Martin, N.F., Irwin, M., Chapman, S., Ferguson, A.M.N., Lewis, G.F., & McConnachie, A.W. *ApJ*, 671, 1591
 McConnachie, A.W., Irwin, M.J., Ibata, R.A., Ferguson, A.M.N., Lewis, G.F., & Tanvir, N. 2003, *MNRAS*, 343, 1335
 Riess, A., & Mack, J. 2005, in *Instrument Science Report ACS 2004-006*
 Stetson, P. 1987, *PASP*, 99, 191